Electrode interface polarization formation in dielectric elastomer actuators

Iannarelli, Alessandro; Ghaffarian Niasar, Mohamad; Ross, Rob

DOI
10.1016/j.sna.2020.111992

Publication date
2020

Document Version
Final published version

Published in
Sensors and Actuators, A: Physical

Sensors and Actuators A 312 (2020) 111992

Contents lists available at ScienceDirect

Sensors and Actuators A: Physical

journal homepage: www.elsevier.com/locate/sna

Electrode interface polarization formation in dielectric elastomer actuators

Alessandro Iannarelli*, Mohamad Ghaffarian Niasar, Rob Ross

DC Systems, Energy Conversion and Storage, Faculty of Electrical Engineering, Mathematics and Computer Science, Delft University of Technology, Mekelweg 4, 2628 CD Delft, The Netherlands

ARTICLE INFO

Article history:
Received 23 December 2019
Received in revised form 31 March 2020
Accepted 31 March 2020
Available online 5 May 2020

Keywords:
DIelectric elastomer actuators
Dielectric spectroscopy
Electrode polarization
Reliability
Space charges
Interface polarization
Electroactive polymers

ABSTRACT

Dielectric elastomer actuators (DEAs) are a class of electrostatic actuators that have promising applications in fields like sensors, soft-robotics, microfluidics, and energy harvesting. The crucial points in the working principle of DEA are the application of high electric field and the use of compliant electrodes. These electrodes are typically composed of a mixture of a soft polymer base filled with highly conductive particles. In this work, we show that the charged impurities, possibly present in the electrodes composite, in combination with a high electric field can cause the formation of polarization interface layers between the electrodes and the inner dielectric. These layers can, in the long term, diminish the actuation performance of the DEA.

1. Introduction

Dielectric elastomer actuators (DEAs) are a specific class of electroactive polymer (EAP) transducers that exploits the electrostatic force exerted between two conductors to perform a displacement. Because of their pliability, high efficiency, noiseless operation, and fast electromechanical response [1–4] they are suitable for various application such as artificial muscles, robotics, optics, sensors, microfluidics, and energy harvesting [5–14] and received attention in commercial applications [15].

Despite their versatile properties, DEAs exhibit two main operational disadvantages: the need for flexible electrodes and high electric fields [16]. Manufacturing electrodes with high compliance and conductivity represents a challenging task as the two properties are often mutually exclusive [17]. Whereas, the intrinsically low permittivity ε of elastomers makes necessary the use of a relatively large electric field E_z for a sufficient actuation force F_z. This follows from the relation:

$$F_z = \varepsilon A {E_z}^2 = \varepsilon A \left(\frac{V}{d}\right)^2 \quad (1)$$

where A is the electrode area. In the right-hand side of the equation, the field E_z is re-written in terms of the applied voltage V and the elastomer thickness d. A high electric field can, thus, be obtained either by reducing the dielectric thickness or using a substantial voltage potential [18].

To overcome these disadvantages, compliant electrodes are typically prepared with highly doped elastomer composites [19–24] and inorganic fillers are used to artificially augment the dielectric's permittivity [25–31] as well as the chemical functionalization of the elastomer [32].

Despite the efforts, still typically high electric field strengths need to be involved for a significant actuation displacement. The influence of high electric fields (or voltages) on the dielectric properties of DEA system is scarcely investigated as most of the research is performed at low voltages [33]. In the presence of strong electric fields, new phenomena can establish and drastically impact the dielectric properties. A distinctive example is given by the formation of space charges (SC) at low-frequency high fields [34,35].

Space charges formation in dielectrics exposed to high DC voltages is a known effect for polymeric materials used in DEAs fabrication [36–40]. However, the evolution of SC at the electrodes–dielectric interfaces and its consequences on the DEA actuation performance are much less studied.

Our research investigates the dielectric phenomena at the interfaces. Specifically, we studied through dielectric spectroscopy (DS)

* Corresponding author.
E-mail address: a.iannarelli@tudelft.nl (A. Iannarelli).

https://doi.org/10.1016/j.sna.2020.111992

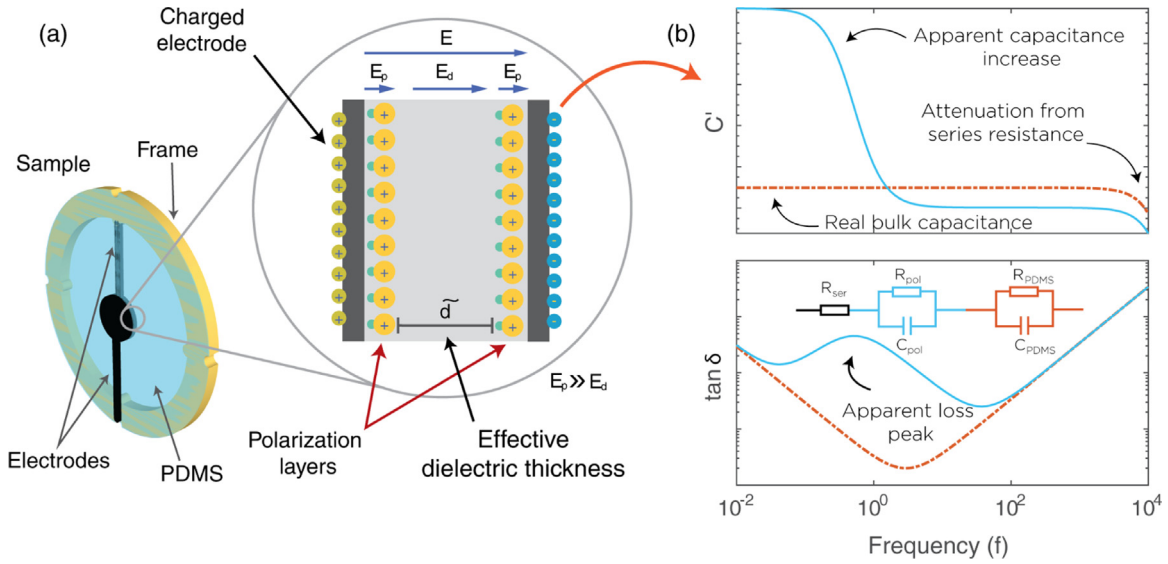

Fig. 1. Schematic representation of the space charge formation at the interface. (a) Sample pan view. In the inset, the formation of the electrode polarization layers happens at the electrode-dielectric interfaces (b) Consequences of electrode polarization layers on real capacitance and dielectric losses (tan δ) spectrum. These layers result in a parasitic capacitance C_{pol}, that adds to and modify the pre-existing dielectric capacitance C_{PDMS}.

how the charged impurities migrating from the doped electrodes (forced by the high electric field employed) can form polarization layers at the electrodes/dielectric interfaces. Successively, we observed the consequences of these charged layers formation on the mechanical capabilities of the DEA system by monitoring its actuation performance over time.

The first part of this work presents the equivalent electrical model used to describe the interface phenomenon. The second part addresses the results about space charge measurement performed with dielectric spectroscopy and the performance characterization over time of DEA.

2. Dielectric phenomena at interface of DEAs

Compliant electrodes used in DEAs are typically composite materials. They are prepared by adding highly conductive fillers (e.g. metal particles, carbon blacks, ionic gels, dopants) to an elastomer base material until the percolation threshold is reached [22,19]. Depending on the fabrication method used, these composites can contain ionic impurities as well as free ions resulting from residual catalysts, solvents or the filler themselves [41,42]. Under the influence of a sufficiently high electric field, these impurities are pushed across the electrode-dielectric interface (see Fig. 1(a)) leading to the development of a charged accumulation layer [43]. This phenomenon is known as electrode polarization (EP) [44]. The resultant capacitance of these parasitic layers superimposes to the real sample capacitance. Because of the large inertia of the impurities, the effect is dominant at low frequency, i.e. when they are slowly accelerated and exposed to a unipolar field for a longer time. As a result, the capacitance superimposition can be observed via dielectric spectroscopy as a low-frequency signal enhancement, Fig. (1 (b)).

When an external voltage is applied, the presence of the parasitic layer modifies the internal electric field distribution. A part of the applied electric field concentrates next to the interfaces and the remaining part in the bulk. This unwanted effect is a common problem in electrochemistry field [45] because it disguises the dielectric contribution of the actual sample. In the case of DEA, however, its presence can be used to assess the actuator performance over time and its reliability.

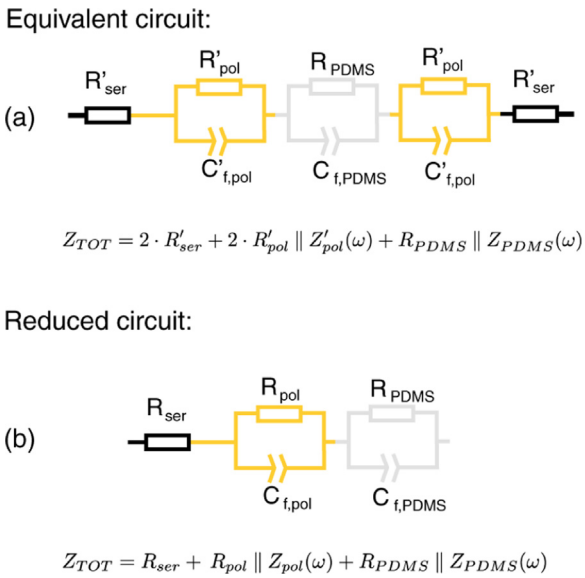

Fig. 2. Total impedance Z_{TOT} model of DEA using lumped elements. Both the interfaces and the dielectric bulk are described by the constant phase elements impedances $C_{f,pol}$ and $C_{f,PDMS}$ in parallel with the respective resistive elements R'_{pol} and R_{PDMS}. The electrodes are modeled as two pure resistive elements R'_{ser}. Due to symmetry, the equivalent circuit can be re-written in a reduced form (bottom equation).

2.1. Interface modeling

To investigate the formation of the space charges at the interface, we construct an equivalent electrical circuit to fit the experimental impedance spectra obtained via dielectric spectroscopy, Fig. 2 [46]. We emulate the parasitic and sample capacitances using constant phase elements (CPE). The CPE is specifically suitable to describe interface effects [47,48]. It is characterized by the two parameters α and C_{CPE}

$$Z_{CPE} = \frac{1}{(j\omega)^{\alpha} \cdot C_{CPE}}, \qquad \alpha \leq 1 \tag{2}$$

Here $j^2 = -1$ is the imaginary unit and ω is the anglular frequency of the applied signal. The parameter C_{CPE} has the unit of $[C_{CPE}] =$

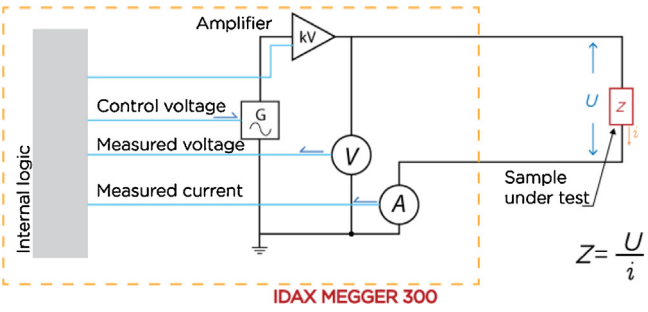

Fig. 3. Minimalistic representation of the dielectric spectrum analyzer. The generated signal and the resulting current are measured. The impedance is calculated as te ratio of the two complex quantities U (voltage) and i (current).

$F \cdot s^{\alpha-1}$. When $\alpha = 1$, C_{CPE} is a capacitance. In this work, we address to the CPE simply as a modified capacitive element with unit $\tilde{pF} = pF \cdot s^{\alpha-1}$.

3. Experimental

3.1. Dielectric spectroscopy

Dielectric spectroscopy (DS) measurements were performed using a Megger Idax 300 Insulation Analyzer unit in combination with the Megger Vax 020 High Voltage Amplifier, Fig. 3. The tests were done in normal environment conditions (20°C an 1 atm). A custom rig was used to hold the samples in place during the test. DS was performed on the samples in three stages: firstly, low-voltage ($V_{peak}^{(LV)} = 10$ V, corresponding to a field $E_{peak}^{(LV)} = 0.19$ kV/mm) DS was performed in the range from 10 mHz to 10 kHz to assess the capacitance baseline of new DEA samples. In the second stage, the DS was executed at high voltage ($V_{peak}^{(HV)} = 1980$ V, hence $E_{peak}^{(HV)} = 37.2$ kV/mm) in a reduced frequency-range from 10 mHz to 2 kHz. The high voltage in this stage has a twofold function: it is needed for the DS spectrum measurement at a higher electric field, and it simultaneously forces the migration of the charged particles at the interfaces. In the third and last stage, the samples were successively re-tested with low voltage at defined time intervals.

The reduced frequency range of the HV test is due to the limitation of the amplifier. It is worth mentioning that the frequency sweep was performed from high to low frequencies in all cases. From non-reported tests, however, we found that the sweep order won't influence the final results.

3.2. Sample preparation

The samples in this analysis were prepared using commercially available Wacker Elastosil Film 2030 polydimethylsiloxane (PDMS) films. The 100 μm thick silicone sheets were cut in discs of 50 mm diameter. A radial stretch of $\lambda_r = 1.5$ was imposed on the resulting membranes by the Open-Source Radial Stretching System (RSS) [49]. To hold the membranes tensioned, these were anchored to rigid ring-shaped polymethylmethacrylate (PMMA) frames of 34 mm inner diameter and 2 *mm* thickness. A double-sided polyamide silicone glue tape was used as fasten layer between the PDMS and the PMMA. The electrodes were then patterned on both sides of the membranes using the spray-paint technique. A conductive and elastic ink [50] was sprayed with an airbrush through shadow masks of proper shape. The ink was prepared by dispersing through a high-speed mixer(Thinky ARE-250) carbon black fillers (Cabot Black Pearl 2000) into an uncured silicone base (Nusil MED-4901). Isopropyl-alcohol and iso-octane were used as thinner for this process. The painted devices were cured in a ventilated oven at 50 °C for 40 min. After this time, contacts were added to the electrodes by painting two silver ink pads (RS PRO Silver Conductive Paint). The device was then put back into the oven for a last curing step of 12 h at 50 °C. The resulting electrodes have a circular shape of 12 mm diameter and an average thickness of 10 μm, measured using the surface profilometer Dektak 150.

The samples preparation was performed in an ISO 7 controlled environment to avoid external particulate contamination.

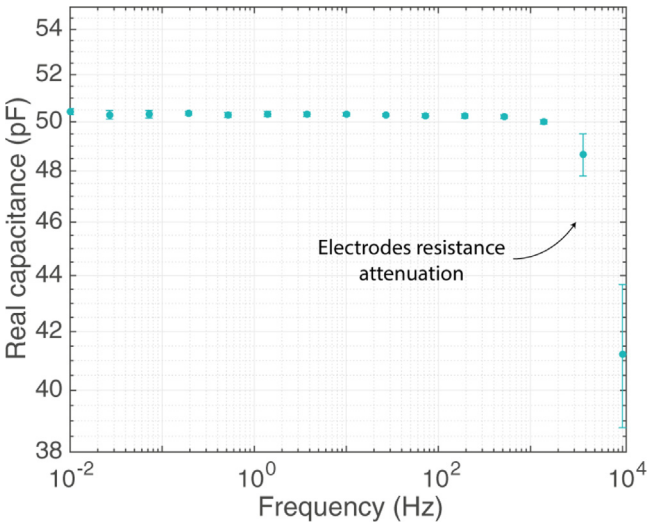

Fig. 4. Real part of the DEA capacitance resulting from the first dielectric spectroscopy stage performed at low voltage, $V_{peak}^{(LV)}$=10 V. The high-frequency decrease is due to the electrodes high resistivity, which makes the system act as an RC filter. The error bars represent the measurements standard deviation over 5 samples.

4. Results and discussion

4.1. Interface polarization

4.1.1. Dielectric spectroscopy at low voltage

The dielectric spectroscopy performed on 5 new DEA samples at low electric field (low voltage) shows the expected behavior of a parallel plate capacitor, Fig. (4). The real part of the capacitance is approximately constant in the whole measured frequency range. In the high frequency ($f > 2$ kHz) tail, the resistive effect of the electrodes becomes predominant. In this region, the system behaves as an RC filter attenuating the flowing current and altering the voltage distribution along the electrode surface [51]. The electrostatic compression for this low voltage is negligible, and there is no valuable capacitance change resulting from it in the dielectric spectroscopy. The measured capacitance in the range from 0 to 500 Hz has an average value of $C_{LV} = 50.26 \pm 0.09$ pF.

4.1.2. Dielectric spectroscopy at high voltage

The DS is successively performed at high voltage $V_{peak}^{(HV)}$ ($E_{peak}^{(HV)}$) on the same samples previously tested at LV. Significant changes appear in the dielectric response of the DEAs, Fig. 5. For their analysis, it is convenient to divide the spectrum in two adjacent regions delimited by the central value $f* = 10$ Hz. The low frequency range $\mathcal{F}_{LF}$ contains frequencies from 10 mHz up to $f* = 10$ Hz, whereas the high frequency range $\mathcal{F}_{HF}$ contains the remaining frequencies above $f*$.

Following the frequency-sweep direction, i.e. from high to low, it is observed a capacitance increase with decreasing frequency of about 1 pF in the $\mathcal{F}_{HF}$ range with respect to the previous low voltage measurements. The decrease corresponds to about 2% enhance-

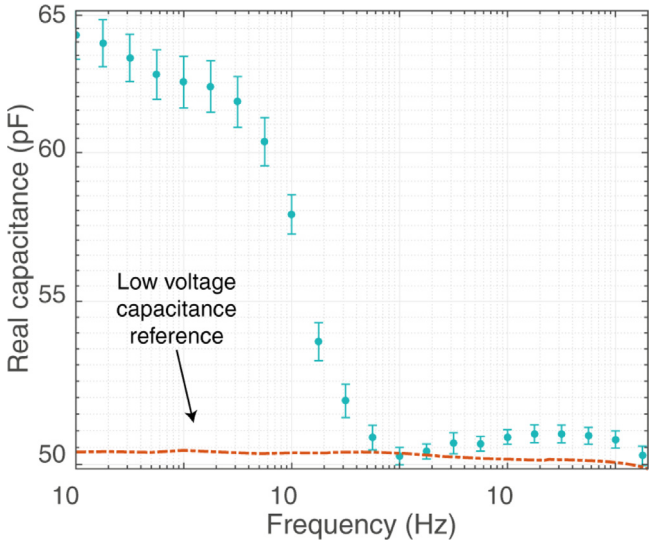

Fig. 5. Real part of the DEA capacitance resulting from the second dielectric spectroscopy stage performed at high voltage, i.e. $V_{peak}^{(HV)} = 2$ kV. A noticeable increase of capacitance is visible for frequencies lower than $f* = 10$ Hz.The error bars represent the measurements standard deviation over 5 samples. The low voltage average value (dashed line) is also reported for reference.

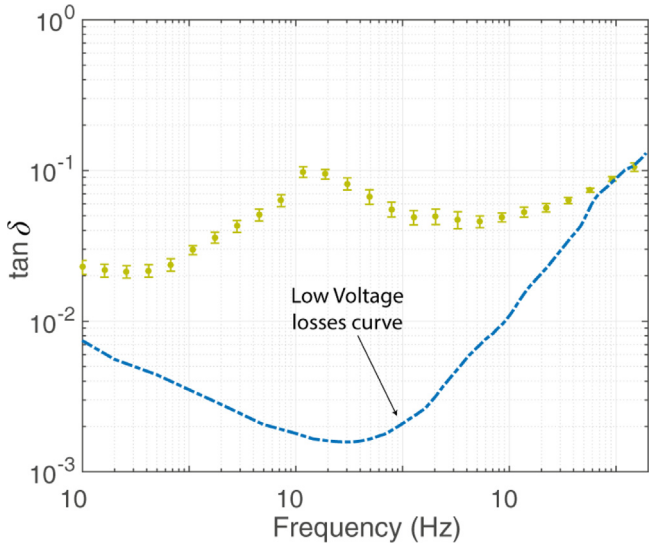

Fig. 6. tanδ measurement of the second dielectric spectroscopy stage performed at $V_{peak}^{(HV)} = 2$ kV. The peak is located around 1.45 Hz. The error bars represent the measurements standard deviation over 5 samples. It is visible the large difference with the low voltage losses (dashed line).

ment of the original capacitance. The values in this range show small scattering and hence a uniform change for all the samples.

Continuing on the lower frequencies of $f*$, instead, a steep capacitance increase appears. The capacitance values keep monotonically increasing with decreasing frequencies, with a milder slope from 500 mHz to 10 mHz. The scattering of the values is larger in this range, with a standard deviation of $\sigma_{LF,HV} = 2.2$ *pF*. Large variations are present in the measurement of tan δ, i.e. the medium's dielectric losses, Fig. 6. More than an order of magnitude of additional losses are measured for frequencies lower than about 100 Hz. All the measurements show a peak value of around 1.45 Hz.

At higher frequencies, the tan δ behavior is dominated by the contribution of the resistive electrodes used. In contrast, for lower

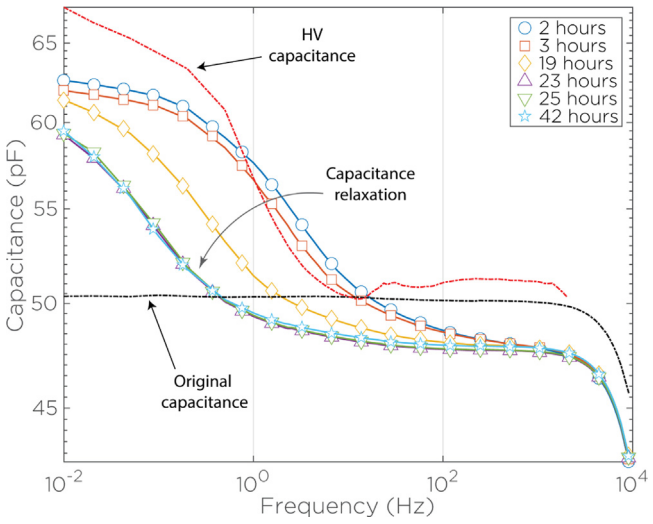

Fig. 7. Real part capacitance evolution over time measured in the third stage of dielectric spectroscopy. The high voltage (dashed red line) and low voltage (dashed black line) are reported for comparison. All the tests are performed at the low voltage $V_{peak}^{(LV)} = 10$ V. No voltage is applied to the samples between two consecutive measurements.

frequencies, we observe the contribution of the PDMS and its interfaces with the electrodes.

The capacitance enhancement recorded in $\mathcal{F}_{HF}$, is explained by the membrane thinning, which results from the electromechanical action of the electrodes. In the presence of high electric fields, the electrostatic force causes a significant compression. From the well known parallel-plate capacitor relation

$$C = \frac{\varepsilon_0 \varepsilon_r A}{d} \tag{3}$$

(where A is the area of the electrodes) it is readily understood that a decrease in thickness causes a capacitance increment. In principle, this same argument could be used to explain the behavior in $\mathcal{F}_{HF}$. It could be argued that at low frequency, the sample can compress more, because of a less viscoelastic effect and therefore, an even more considerable capacitance increase could follow. The last hypothesis is proved to be contradicted by the outcomes of the next Section 4.1.3.

4.1.3. Dielectric spectroscopy evolution over time

The DS was repeated on the same samples at low voltage after the HV investigation, Fig. (7). A persistent capacitance increase for frequency in the range $\mathcal{F}_{LF}$ is still measured. Such a trend was not encountered in the previous low voltage measurements shown in Fig. (4). But, it was recorded for the first time under high voltage conditions, Fig. (5).

The compression argument exploited to explain the capacitance increase in $\mathcal{F}_{HF}$ (Section 4.1.2), cannot hold in this case because the induced displacement at low voltage is reasonably negligible. Also, the capacitance measured in $\mathcal{F}_{HF}$ are in this case lower than the baseline by approximately 2 pF.

The two phenomena together indicate that the high electric field imposed during the high voltage DS changed the DEAs properties under test. These results showed to be reproducible for all the samples tested in a coherent manner. The samples were left apart in controlled temperature conditions (20 degree Celsius) and were re-tested with low voltage at successive time intervals to assess the stability of the changes. The curves in Fig. 7 show the time evolution of the observed capacitance for a representative specimen.

Right after the high voltage application, the low voltage DS still registers high capacitance values in the $\mathcal{F}_{LF}$ range. These values reduce over time. After about 23 h the samples were put in an oven

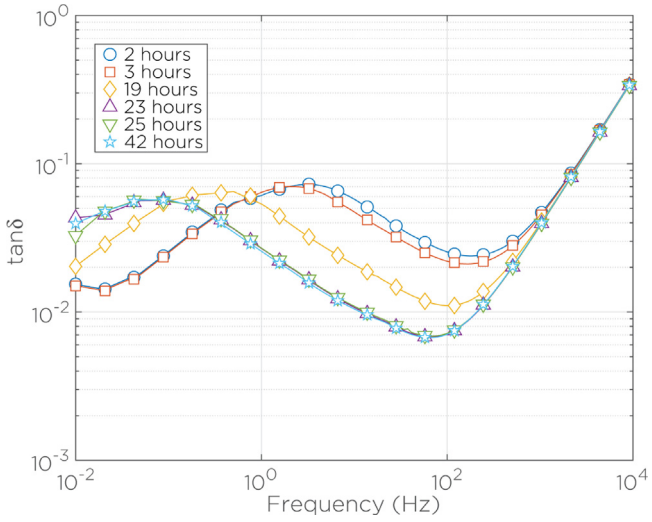

Fig. 8. Evolution of tanδ over time measured at the third stage dielectric spectroscopy at low voltage. The central peak shifts leftwards over time because of the gradual reduction of the polarization layers in absence of an external electric field.

at 50 °C for two hours and tested again once cooled down to room temperature. After 42 h no difference in the curves was noticeable anymore.

An equivalent time evolution can be observed also for the tan δ measurement, as shown in Fig. 8. The central peak ($f_{peak}(t = 0) =$ 3.6 Hz), which appeared with the high voltage application, shifts to lower frequency with the time passing. After the 42 hours period, it stabilizes to its final position ($f_{peak}(t = 42\,h) = 7.5$ mHz).

4.1.4. Inception threshold

The DS was performed at successively high voltage levels on untested samples to measure the electric field threshold for the inception of the polarization effect. Namely, this is the threshold above which a permanent dielectric change is observable in the DEA system.

Ten voltage-peak levels logarithmically-spaced between 198 V and 1980 V were chosen for the test. In Fig. 9, six of these voltage level results are reported. A mild capacitance increase due to polarization is visible at lower voltages for frequencies less than 100 mHz. For voltages up to 711 V (about 13 kV/mm nominal electric field), the real part of the capacitance stays nearly unchanged, Fig. 9(a). As the voltage reaches around 918 V peak (or about 16 kV/mm nominal electric field), a sudden increase is observed which persists for higher voltages (electric fields). An analogous change is observed in the dielectric losses investigation for the same voltage, Fig. 9(b). In this figure, the formation of a hump is observed between the two voltages 918 V and 1187 V. The phenomenon can also be observed in a Nyquist plot for the capacitance values. When the polarization sets, the respective curves bend till forming arc-like curves at lower frequencies, as can be observed in the curves in Fig. 9(c).

The value $E_{th} = 16$ kV/mm is therefore considered the electric field threshold for the injection of permanent polarization layer for this specific system.

4.1.5. Lumped model fitting

The permanent dielectric variation is explained by the formation of space charges at the interfaces during the high voltage stage of DS. The impurities contained in the electrodes, moved towards the interface, creating a stable polarization layer.

The polarization layers are schematized using the lumped model presented in Section 2.1 and showed in Fig. 2. Both the PDMS bulk and the interfaces are modeled with the CPE elements $C_{f,PDMS}$ and $C_{f,pol}$. Parallel to the CPEs, the parasitic resistances R_{PDMS} and R_{pol} are included to account for the material and interface losses, respectively.

The total impedance Z_{TOT} measured through dielectric spectroscopy in Section 4.1.3 has been fitted with this lumped model using the MEISP 3.0 (Multiple Electrochemical Impedance Spectra Parameterization) software by Kumho Chemical Laboratories. The results are showed in Fig. (10). The evaluated fit parameters of the impedance data to the equivalent circuit are reported in Table (1).

We can track the time evolution of the charged interface: initially, as the polarization layer is formed, it is characterized by a large capacitance $C_{f,pol}$. At the same time, a large capacitance $C_{f,PDMS}$ relative to the PDMS bulk is measured. Comparing this value to the initial $C_{0,LV}$ is evident a large enhancement. This is explained by the reduced PDMS effective thickness $\tilde{d}$. Over time, the value of $C_{f,pol}$ gradually decreases: the formed charges start diffusing and recombining, shrinking the interface layer depth. The PDMS capacitance $C_{f,PDMS}$ diminishes accordingly: the effective PDMS thickness $\tilde{d}$ is now increasing.

We can finally compare the evolution of the tan δ peaks which appear in the $\mathcal{F}_{LF}$ range. According to the proposed lumped model this are roughly proportional to the ratio

$$\propto \frac{1}{C_{\alpha,1} \cdot R_{pol}}$$

We compared these values with the ones actually measured over the time evolution, and we reported them in Table (2). In all the cases there is a direct proportionality k between the estimated values by the model and the actual measured ones. This is a further confirmation of the validity of our fit.

4.1.6. Comparison with other materials and conditions

The three-stages-dielectric-spectroscopy test was performed on different materials to assess the formation of polarization layers. Two rigid polymers films, namely low-density polyethylene (LDPE) and polyvinyl chloride (PVC), were tested using the same sample preparation method exploited in the PDMS case. Due to the stiffness of LDPE and PVC, no pre-stretch was applied to these samples. The measured film thicknesses were 103 μm and 160 μm for the LDPE and PVC, respectively. The high voltage $V_{peak}^{(HV)}$ used for the high-voltage dielectric spectroscopy stage has been chosen to have the resulting respective electric field E, such that $E > E_{th}$. The value $E_{th} = 16$ kV/mm is the electric field threshold measured for the PDMS-based DEA.

As can be seen from Fig. 11, these materials show similar behavior to the PDMS case. At low voltage, both LDPE and PVC exhibit only bulk polarization [52]. During the second stage DS, performed under the high electric field E, the EP settles and persists even after the high voltage is removed. The polarization persistence can be observed in the third and last stage of DS, which is performed again at low voltage.

A final test was conducted on PDMS using non-compliant, pure aluminium electrodes. The rigid aluminium prevents the presence of impurities or free ions that can form the EP layer, like in the case of the carbon-silicone composite. The peak voltage was gradually increased up to $V_{peak}^{(HV)} = 1980$ V and then reverted back to low voltage. The results (see Fig. 12) show that, with this configuration, no permanent polarization layer is formed during the HV phase. A minor capacitance increase all over the spectrum is explained by the electrostatic force squeezing the silicone layer, thus reducing its thickness, Eq. (3). When re-testing at low voltage, the sample recovers its original capacitance showing the absence of permanent EP.

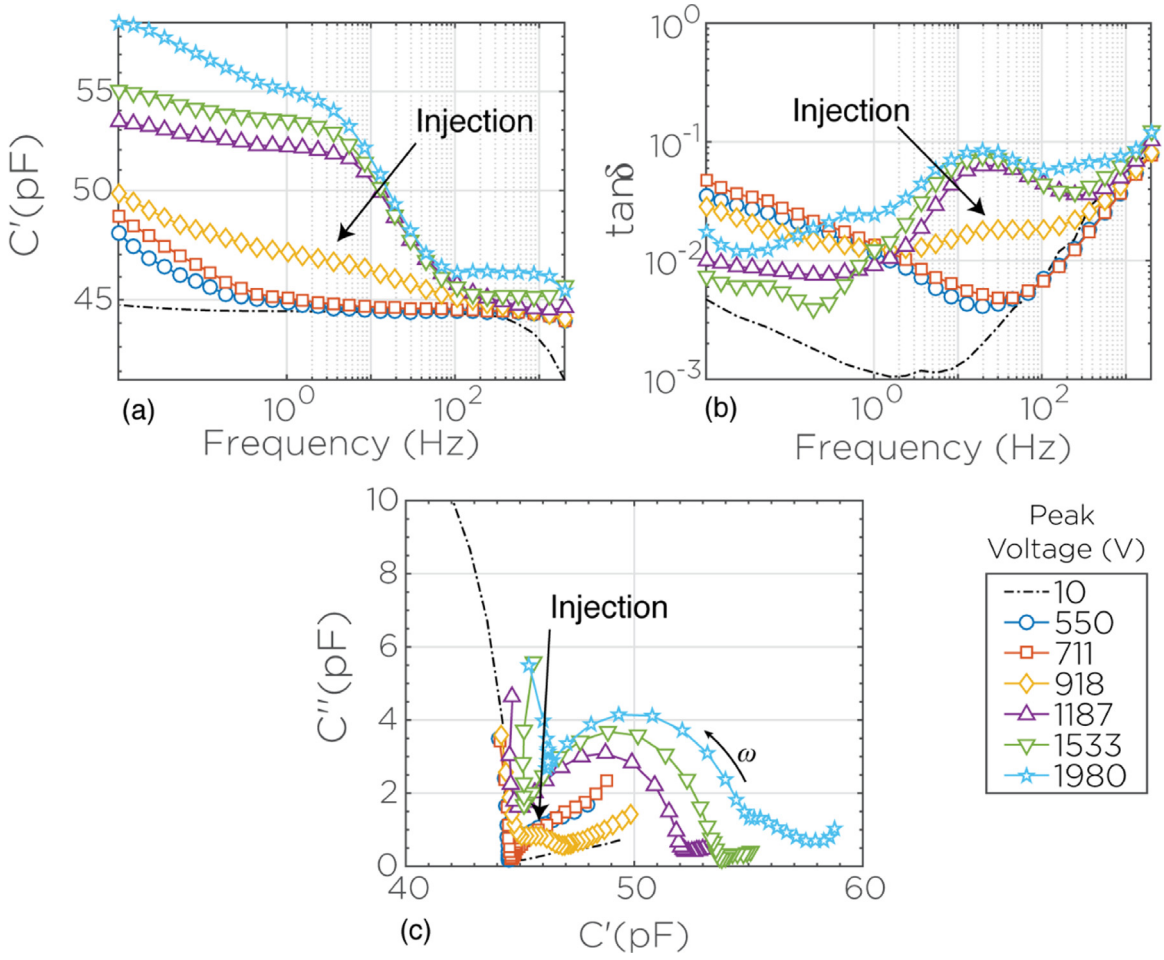

Fig. 9. Polarization injection study compared with the low voltage baseline measurement. (a) Capacitance frequency-sweeps. (b) tanδ dielectric loss measurement. (c) Nyquist plot of the capacitance, the arrow indicates the direction of increasing frequency ω; the formation of a new arc in the curves is noticeable as the polarization settles.

Table 1
Time evolving fit-parameters resulting from the lumped model for the DEA actuator.

Time	$R_{ser}(\Omega)$	$C_{f,pol}(\tilde{pF})$	α_{pol}	$R_{pol}(\Omega)$	$C_{f,PDMS}(\tilde{pF})$	α_{PDMS}	$R_{PDMS}(\Omega)$
t_0	11.64×10^4	401.7	0.9984	1.14×10^7	60.17	0.99	1.86×10^{14}
t_1	11.16×10^4	395.1	0.9983	1.59×10^8	59.72	0.99	1.85×10^{14}
t_2	11.79×10^4	331.5	0.9961	1.00×10^9	59.22	0.9941	1.85×10^{14}
t_3	11.92×10^4	318.6	0.9962	3.83×10^9	58.07	0.9964	1.85×10^{14}
t_4	11.93×10^4	315.1	0.9941	3.80×10^9	58.23	0.9968	1.85×10^{14}
t_5	12.03×10^4	321.5	0.9957	4.19×10^9	58.25	0.9965	1.8×10^{14}

The tests together show that the measured EP is independent by choice of the dielectric medium, but rather depends on the electrodes used. Explicitly, it confirms that a high concentration of impurities or unbonded charges contained in the conductive carbon-silicone composites used as electrodes can promote the EP formation.

Finally, these results encourage the use of pure metal electrodes for the future development of interface-polarization-free DEAs. For example, it has been recently shown [53] that gold can covalently bond to thiol-functionalized silicone (SH-PDMS) surface to form an ions-free compliant conductive layer.

4.2. Actuation effects

The polarization effects were measured on the actuation performance of the DEA over time. Two sets of samples were continuously actuated with 1 Hz square and sine wave AC 4 kV peak voltage, respectively. From results of Section 4.1.4, this voltage ensures the creation of polarization at interfaces. Both sets were video-recorded for the entire length of the test. Afterwards, the information about the radius change was extrapolated from the recordings with the aid of custom MATLAB code.

Fig. 13(a) shows how the relative actuation stroke $s_{\%}(t)$ defined as

$$s_{\%}(t) = 100 \times \frac{r_{ON}(t) - r_{OFF}(t)}{r_{ON}^{(0)} - r_{OFF}^{(0)}} \tag{4}$$

where r is the measured radius, diminishes over time. The ON-(OFF-)radius is defined as the maximum (minimum) radius measured over a voltage cycle.

The highest performance loss (in terms of actuation stroke) is measured for the AC sine wave case. The formed charged layers, concentrate the electric field at the interfaces attenuating the bulk electric field responsible for the compression. As a consequence,

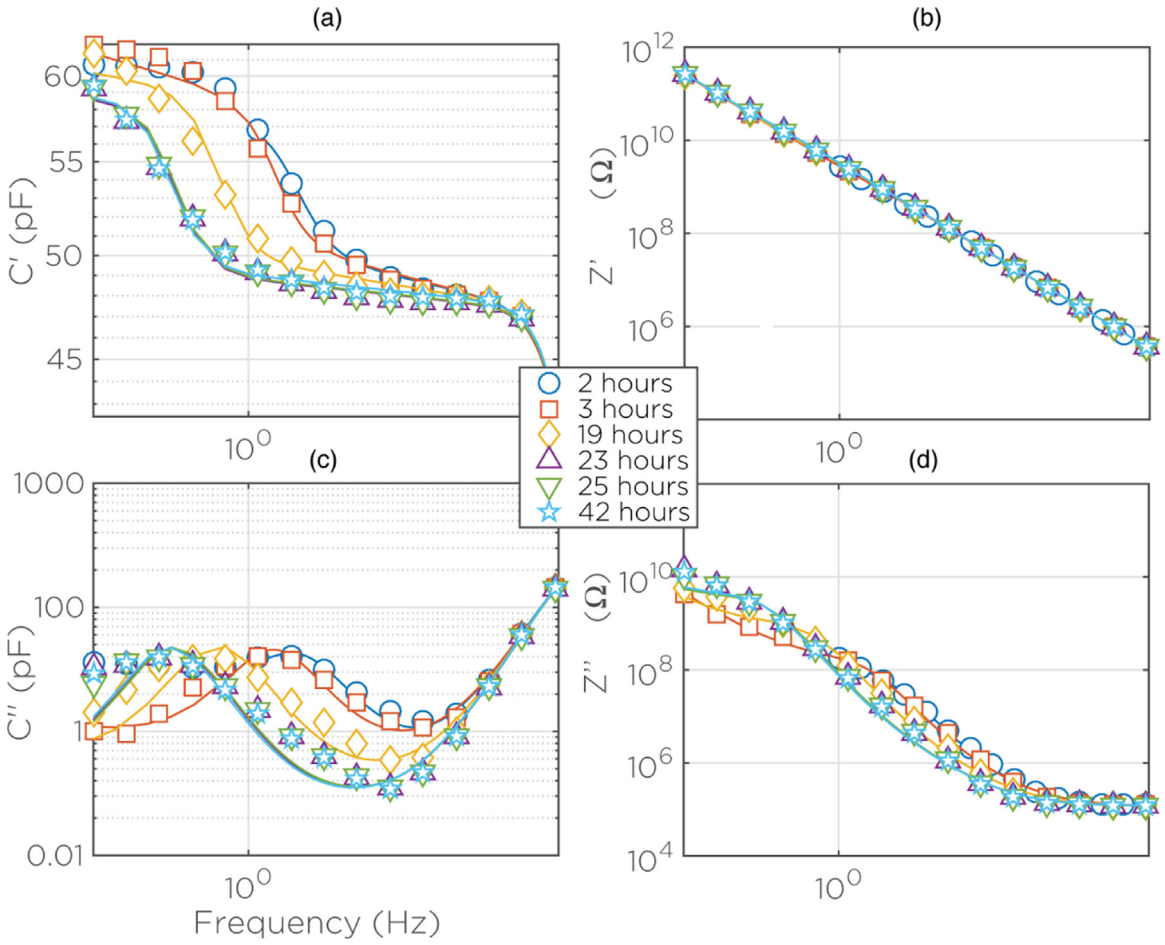

Fig. 10. Fitting of the time evolving total capacitance $C = C' + iC''$ and impedance $Z = Z' + iZ''$ with the proposed lumped model including constant phase elements. (a–c) Real and imaginary capacitance fitting. (b–d) Real and imaginary impedance fitting. Solid lines represent the fitting of the data points, represented by the markers.

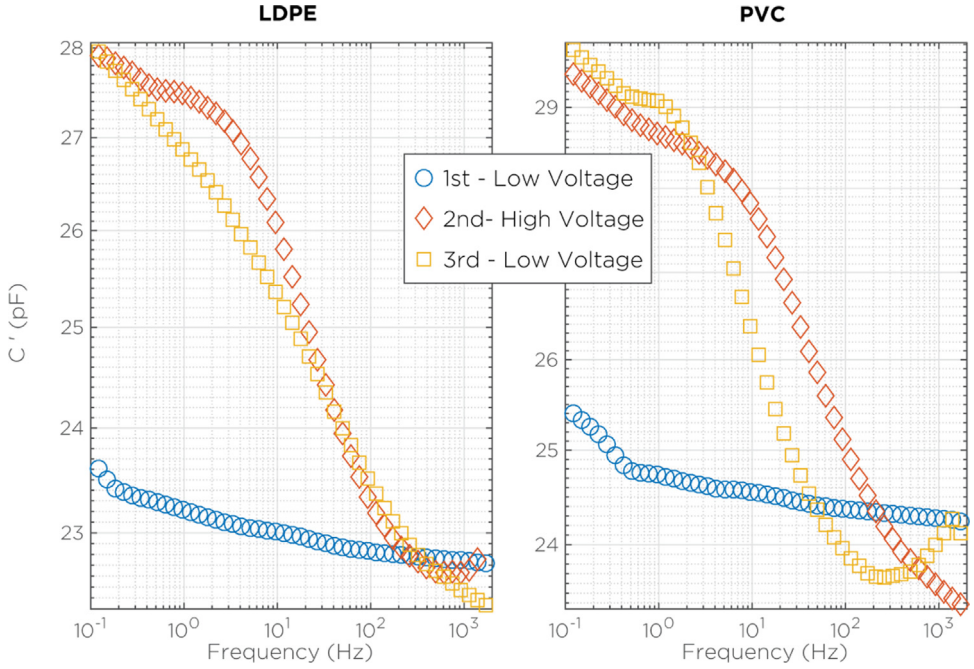

Fig. 11. Capacitance measurements resulting from the three stages dielectric spectroscopy performed on LDPE (left) and PVC(right). The initial low-frequency capacitance enhancement for the low voltage curves is due to the bulk polarizability.

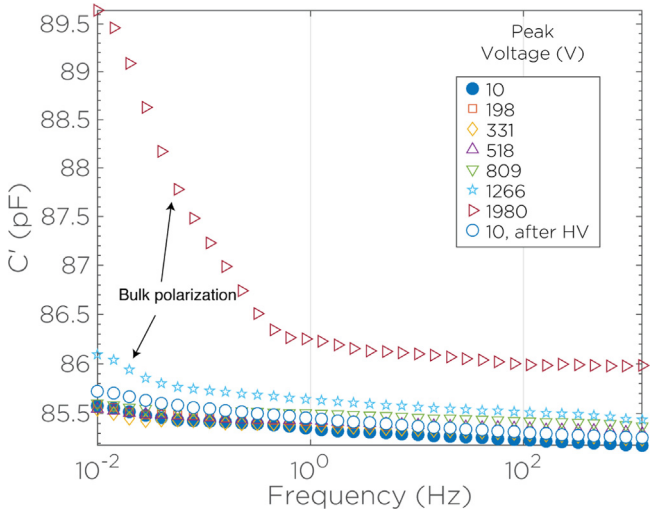

Fig. 12. Capacitance measurement on PDMS film using rigid aluminium electrodes. The electrodes radius is in this case slightly larger than the CB-PDMS and a higher capacitance is thus recorded. A reversible bulk polarization of the PDMS is visible for lower frequencies.

the available electrostatic pressure in the bulk is reduced as well as the resulting displacement.

The ON-radius reduces over time because the bulk electric field, which causes the compression, reduces with the charged interface formation, Figs. 13(*b*)-(*c*) (dark lines).

Similarly, in the OFF state, the growing permanent polarization charges settle an electric field that holds the compression and prevents the DEA to recover to its initial unperturbed state fully. This explains the increasing radius in the OFF state, Figs. 13(*b*)-(*c*)(bright lines).

Table 2
Frequency-location of the tanδ peak fitting results.

Time	$f_0(Hz)$	$(C_{f,pol} \cdot R_{pol})^{-1}$	k
t_0	3.05	24.67	8.09
t_1	1.92	15.83	8.24
t_2	0.35	3.01	8.61
t_3	0.1	0.81	8.18
t_4	0.1	0.83	8.3
t_5	0.1	0.74	7.4

It was observed that the process is, to a certain extent, reversible: by shorting the actuators electrodes for a long period of time (>24 h), they were able to actuate again to nearly the same initial stroke.

5. Conclusions

This study aimed to assess the polarization charges creation at the electrodes-insulator interface and to measure its effects on the actuation performance of a dielectric elastomer actuator (DEA) systems. Dielectric spectroscopy (DS) was performed on the sample in three stages. A systematic and permanent capacitance increase was measured when exposing the sample to low frequency (<10 Hz) and high-intensity electric fields (>16 kV/mm). The result was attributed to the creation of space charges at interfaces. An equivalent circuit was modelled to quantify the interface polarization mechanism, and it successfully fitted the experimental data.

The effects of the polarization charges were studied on the actuation stroke over time. It was generally observed a stroke reduction over time caused by the formation of polarization charges. The worst performance was measured in the case of AC sine driving signal.

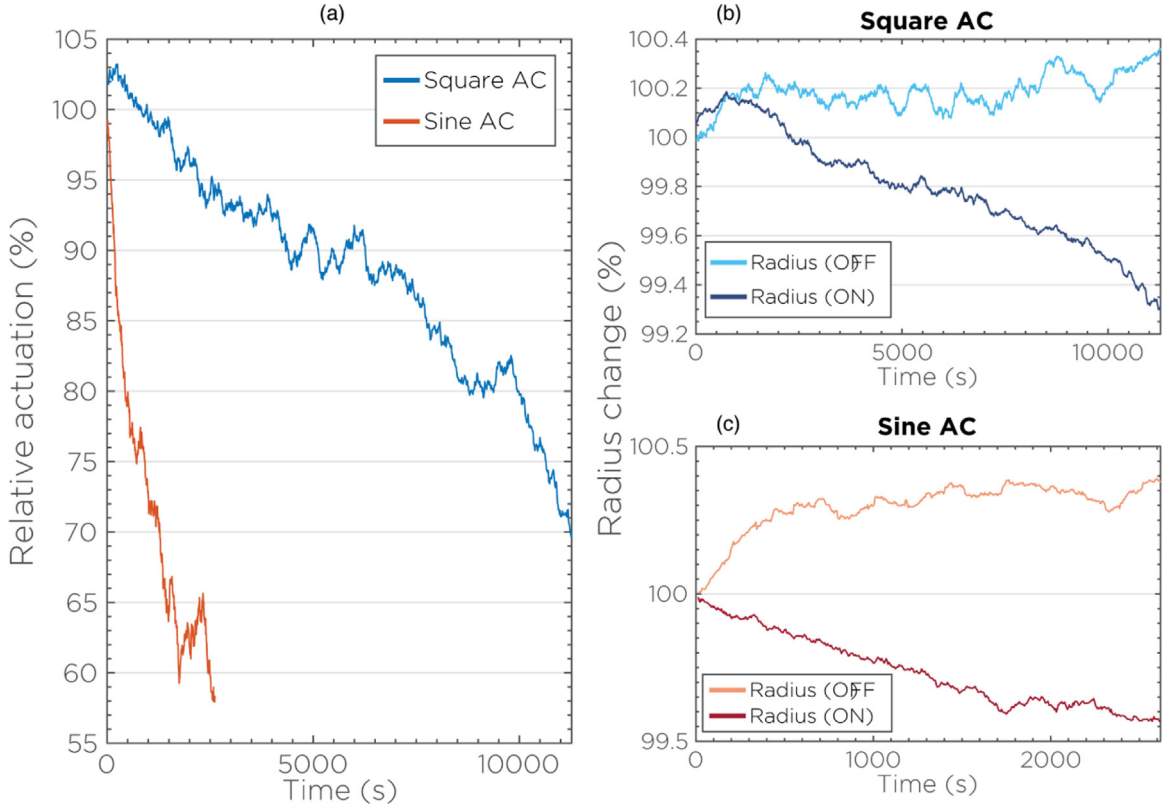

Fig. 13. (a) Relative stroke reduction over time for the two different investigated waveforms. In (b) and (c) it is showed how the radius r_{ON} increases over time whereas r_{OFF} decreases because of the polarization layer formation for the square and sine waves (4 kV at 1 Hz), respectively.

Space charges (interface polarization) can explain the severe reduction of actuator performance over time. It is therefore suggested to make a deliberate choice of the material used during electrodes fabrication, and, in particular, it is suggested to avoid the use of material with significant impurities or ions content.

Credit Author Statement

Alessandro Iannarelli: Conceptualization, Methodology, Software, Validation, Formal Analysis, Investigation, Data Curation, Writing- Original draft preparation.

Mohamad Ghaffarian Niasarh.: Investigation, Data Curation, Resources, Writing - Review & Editing.

Rob Ross: Visualization, Supervision, Writing - Review & Editing, Project administration

Acknowledgements

This work was possible thanks to the financial of Marie Sklodowska-Curie Innovative Training Network (MSCA-ITN-2014-ETN) grant 641822.

References

[1] K. Jia, T. Lu, T. Wang, Response time and dynamic range for a dielectric elastomer actuator, Sens. Actuators A: Physical 239 (2016 mar) 8–17.
[2] P. Maiolino, F. Galantini, F. Mastrogiovanni, G. Gallone, G. Cannata, F. Carpi, Soft dielectrics for capacitive sensing in robot skins: Performance of different elastomer types, Sens. Actuators A: Phys. 226 (2015 may) 37–47.
[3] S.S. Nakshatharan, U. Johanson, A. Punning, A. Aabloo, Modeling, fabrication, and characterization of motion platform actuated by carbon polymer soft actuator, Sens. Actuators A: Phys. 283 (2018 nov) 87–97.
[4] G.Y. Gu, J. Zhu, L.-M. Zhu, X. Zhu, A survey on dielectric elastomer actuators for soft robots, Bioinspiration Biomimetics 12 (2017 jan) 011003.
[5] C. Tang, B. Li, H. Fang, Z. Li, H. Chen, A speedy, amphibian, robotic cube: Resonance actuation by a dielectric elastomer, Sens. Actuators A: Phys. 270 (2018 feb) 1–7.
[6] M. Follador, F. Tramacere, B. Mazzolai, Dielectric elastomer actuators for octopus inspired suction cups, Bioinspiration Biomimetics 9 (2014 sep) 046002.
[7] I.A. Anderson, T.A. Gisby, T.G. McKay, B.M. O'Brien, E.P. Calius, Multi-functional dielectric elastomer artificial muscles for soft and smart machines, J. Appl. Phys. 112 (2012 aug) 041101.
[8] C.T. Nguyen, H. Phung, T.D. Nguyen, C. Lee, U. Kim, D. Lee, H. Moon, J. Koo, J. do Nam, H.R. Choi, A small biomimetic quadruped robot driven by multistacked dielectric elastomer actuators, Smart Mater. Struct. 23 (2014 apr) 065005.
[9] S. Shian, R.M. Diebold, D.R. Clarke, Tunable lenses using transparent dielectric elastomer actuators, Optics Express 21 (2013) 8669–8676.
[10] X. Ji, S. Rosset, H.R. Shea, Soft tunable diffractive optics with multifunctional transparent electrodes enabling integrated actuation, Appl. Phys. Lett. 109 (2016 nov) 191901.
[11] M. Duduta, D.R. Clarke, R.J. Wood, A high speed soft robot based on dielectric elastomer actuators, 2017 IEEE International Conference on Robotics and Automation (ICRA), (Piscataway, New Jersey) (2017 may) 4346–4351.
[12] F.A.M. Ghazali, C.K. Mah, A. AbuZaiter, P.S. Chee, M.S.M. Ali, Soft dielectric elastomer actuator micropump, Sens. Actuators A: Phys. 263 (2017 aug) 276–284.
[13] A. Charalambides, S. Bergbreiter, Rapid manufacturing of mechanoreceptive skins for slip detection in robotic grasping, Adv. Mater. Technol. 2 (2017 nov) 1600188.
[14] R. van Kessel, B. Czech, P. Bauer, Energy harvesting using dielectric elastomers, in 2012 IEEE Power and Energy Society General Meeting (2012 jul) 1–8.
[15] A. Behboodi, S.C.K. Lee, Benchmarking of a commercially available stacked dielectric elastomer as an alternative actuator for rehabilitation robotic exoskeletons, IEEE 16th International Conference on Rehabilitation Robotics (ICORR), (Toronto, ON, Canada) (2019) 499–505.
[16] R. Pelrine, R. Kornbluh, Q. Pei, J. Joseph, High-speed electrically 287 (2000 feb) 836–839.
[17] D. McCoul, W. Hu, M. Gao, V. Mehta, Q. Pei, Recent advances in stretchable and transparent electronic materials, Adv. Electron. Mater. 2 (2016 mar) 1500407.
[18] T. Töpper, F. Weiss, B. Osmani, C. Bippes, V. Leung, B. Müller, Siloxane-based thin films for biomimetic low-voltage dielectric actuators, Sens. Actuators A: Phys. 233 (2015 sep) 32–41.
[19] S. Rosset, H.R. Shea, Flexible and stretchable electrodes for dielectric elastomer actuators, Appl. Phys. A 110 (2012) 281–307.
[20] M. Bozlar, C. Punckt, S. Korkut, J. Zhu, C.C. Foo, Z. Suo, I.A. Aksay, Dielectric elastomer actuators with elastomeric electrodes, Appl. Phys. Lett. 101 (2012 aug) 091907.
[21] Y.R. Lee, H. Kwon, D.H. Lee, B.Y. Lee, Highly flexible and transparent dielectric elastomer actuators using silver nanowire and carbon nanotube hybrid electrodes, Soft Matter 13 (37) (2017) 6390–6395.
[22] M. Kujawski, J. Pearse, E. Smela, Elastomers filled with exfoliated graphite as compliant electrodes, Carbon 48 (2010 aug) 2409–2417.
[23] L. Maffli, S. Rosset, M. Ghilardi, F. Carpi, H. Shea, Ultrafast all-polymer electrically tunable silicone lenses, Adv. Funct. Mater. 25 (2015 jan) 1656–1665.
[24] S. Huang, Y. Liu, Y. Zhao, Z. Ren, C.F. Guo, Flexible electronics: Stretchable electrodes and their future, Adv. Functional Mater. 29 (2019 nov) 1805924.
[25] D. Yang, L. Zhang, H. Liu, Y. Dong, Y. Yu, M. Tian, Lead magnesium niobate-filled silicone dielectric elastomer with large actuated strain, J. Appl. Polym. Sci. 125 (2012 jan) 2196–2201.
[26] M.D. Bartlett, A. Fassler, N. Kazem, E.J. Markvicka, P. Mandal, C. Majidi, Stretchable, High-k Dielectric Elastomers through Liquid-Metal Inclusions, Adv. Mater. 28 (2016 may) 3726–3731.
[27] W. Hu, S.N. Zhang, X. Niu, C. Liu, Q. Pei, An aluminum nanoparticle–acrylate copolymer nanocomposite as a dielectric elastomer with a high dielectric constant, J. Mater. Chem. C 2 (9) (2014) 1658–1666.
[28] L. Yu, A.L. Skov, ZnO as a cheap and effective filler for high breakdown strength elastomers, RSC Adv. 7 (72) (2017) 45784–45791.
[29] L. Namitha, M. Sebastian, High permittivity ceramics loaded silicone elastomer composites for flexible electronics applications, Ceram. Int. 43 (2017 feb) 2994–3003.
[30] T. Chen, J. Qiu, K. Zhu, X. He, X. Kang, E. liang Dong, Poly(methyl methacrylate)-functionalized graphene/polyurethane dielectric elastomer composites with superior electric field induced strain, Mater. Lett. 128 (2014 aug) 19–22.
[31] S. Vudayagiri, S. Zakaria, L. Yu, S.S. Hassouneh, M. Benslimane, A.L. Skov, High breakdown-strength composites from liquid silicone rubbers, Smart Mater. Struct. 23 (2014 sep) 105017.
[32] D.M. Opris, Polar elastomers as novel materials for electromechanical actuator applications, Adv. Mater. 30 (2017 dec) 1703678.
[33] T. Vu-Cong, C. Jean-Mistral, A. Sylvestre, Impact of the nature of the compliant electrodes on the dielectric constant of acrylic and silicone electroactive polymers, Smart Mater. Struct. 21 (2012 sep) 105036.
[34] I. Pleşa, P. Noţ ingher, S. Schlögl, C. Sumereder, M. Muhr, Properties of polymer composites used in high-voltage applications, Polymers 8 (2016) 173.
[35] Y. Zhang, Y. Zhou, M. Chen, L. Zhang, X. Zhang, Y. Sha, Electrical tree initiation in silicone rubber under DC and polarity reversal voltages, J. Electrost. 88 (2017) 207–213.
[36] R. Kochetov, I.A. Tsekmes, P.H.F. Morshuis, Electrical conductivity, dielectric response and space charge dynamics of an electroactive polymer with and without nanofiller reinforcement, Smart Mater. Struct. 24 (2015 jun) 075019.
[37] A. Francis, A. Martinez, K. Thompson, K. Burke, J. Zirnheld, Space charge accumulation as a contributor to partial discharge activity in dielectric elastomer actuators under high voltage DC, in 2016 IEEE International Power Modulator and High Voltage Conference (IPMHVC) (2016 jul) 330–335.
[38] Z.H. Shen, J.-J. Wang, X. Zhang, Y. Lin, C.-W. Nan, L.-Q. Chen, Y. Shen, Space charge effects on the dielectric response of polymer nanocomposites, Appl. Phys. Lett. 111 (9) (2017) 092901.
[39] J. Qiang, H. Chen, B. Li, Experimental study on the dielectric properties of polyacrylate dielectric elastomer, Smart Mater. Struct. 21 (2012 jan) 025006.
[40] B. Li, L. Liu, Z. Suo, Extension limit, polarization saturation, and snap-through instability of dielectric elastomers, Int. J. Smart Nano Mater. 2 (2011 apr) 59–67.
[41] Y. Oka, N. Koizumi, Effects of impurity ions on electrical properties of poly(vinylidene fluoride), Polymer J. 14 (1982) 869–876.
[42] C.C. Liu, A. Walters, M. Vannice, Measurement of electrical properties of a carbon black, Carbon 33 (12) (1995) 1699–1708.
[43] M. Ezoe, K. Kuwada, T. Kawashima, "Icsd'01: proceedings of the 2001 ieee 7th international conference on solid dielectrics: June 25-29, 2001, dorint hotel, eindhoven, the netherlands," (Piscataway, N. J), IEEE, 2001, pp. 85–88.
[44] P.B. Ishai, M.S. Talary, A. Caduff, E. Levy, Y. Feldman, Electrode polarization in dielectric measurements: a review, Measure. Sci. Technol. 24 (2013) 102001.
[45] P. Lunkenheimer, A. Loidl, Dielectric spectroscopy on organic charge-transfer salts, J. Phys.: Condensed Matter 27 (2015) 373001.
[46] P.B. Ishai, M.S. Talary, A. Caduff, E. Levy, Y. Feldman, Electrode polarization in dielectric measurements: a review, Measure. Sci. Technol. 24 (2013) 102001.
[47] H. Sun, H. Zhang, S. Liu, N. Ning, L. Zhang, M. Tian, Y. Wang, Interfacial polarization and dielectric properties of aligned carbon nanotubes/polymer composites: The role of molecular polarity, Compos. Sci. Technol. 154 (2018) 145–153.
[48] K.S. Cole, Electric impedance of suspensions of spheres, J. Gen. Physiol. 12 (1928 sep) 29–36.
[49] S.E. Schausberger, R. Kaltseis, M. Drack, U.D. Cakmak, Z. Major, S. Bauer, Cost-efficient open source desktop size radial stretching system with force sensor, IEEE Access 3 (2015) 556–561.
[50] S. Rosset, O.A. Araromi, S. Schlatter, H.R. Shea, Fabrication process of silicone-based dielectric elastomer actuators, J. Visualized Exp. 108 (2016).
[51] A. Iannarelli, M. Ghaffarian Niasar, R. Ross, Frequency-independent breakdown strength of dielectric elastomers under AC stress, Appl. Phys. Lett. 115 (2019) 092904.
[52] Z. Li, Y. Yin, Y. Wang, P. Jiang, The effect of filler concentration on slow polarization in LDPE/SiO2 micro- and nanocomposites, in 2008 International

Symposium on Electrical Insulating Materials (ISEIM 2008) (2008 sep) 307–310.
[53] B. Osmani, T. Töpper, B. Müller, Conducting and stretchable nanometer-thin gold/thiol-functionalized polydimethylsiloxane films, J. Nanophoton. 12 (2018 may) 1–11.

Biographies

Alessandro Iannarelli graduated in nanotechnology engineering at the Polytechnic University of Turin, Italy in 2014. Since 2015, he is involved in research about reliability of dielectric elastomer actuators exposed to large stresses and high electric fields at the DC Systems, Energy Conversion & Storage department of Delft University of technology (TU Delft), The Netherlands.

Mohamad Ghaffarian Niasar was born in Tehran, Iran in 1984. He received the M.Sc. degree from Sharif University of Technology, Tehran, Iran in 2008, and the Ph.D. degree in Electrical Engineering from Royal Institute of Technology (KTH) in Stockholm, Sweden, 2015. He is currently an assistant professor at DC System, Energy Conversion & Storage group in Technical University of Delft, in Netherlands. His main research interests are aging of insulation material, HVDC insulation system, and multiphysics modeling of power components.

Robert Ross is a professor at TU Delft, director of IWO (Institute for Science & Development, Ede), a professor at HAN University of Applied Sciences and an Asset Management Research Strategist at TenneT (TSO in the Netherlands and part of Germany). At KEMA he worked on reliability and post-failure forensic investigations.